

Electromagnetic form factors of the nucleon from the instanton vacuum

Hui-Jae Lee,^{1,*} Yongwoo Choi,^{2,3,†} and Hyun-Chul Kim^{1,2,4,‡}

¹*Department of Physics, Inha University, Incheon 22212, Republic of Korea*

²*Institute of Quantum Science, Inha University, Incheon 22212, Republic of Korea*

³*The Center for High Energy Physics, Kyungpook National University, Daegu 41566, Republic of Korea*

⁴*School of Physics, Korea Institute for Advanced Study (KIAS), Seoul 02455, Republic of Korea*

(Dated: May 27, 2026)

We investigate the electromagnetic form factors of the nucleon within an effective chiral theory derived from the QCD instanton vacuum, taking into account the finite current quark mass. The momentum-dependent dynamical quark mass, generated by the instanton-antiinstanton medium, naturally plays the role of a regulator, so that no additional regularization is required to tame the divergences arising from quark loops. The instanton parameters, the average instanton size $\bar{\rho} = 0.35$ fm and the average interdistance $\bar{R} = 0.86$ fm, together with the dynamical quark mass at zero virtuality $M_0 = 385$ MeV, are all fixed by the saddle-point equation beyond the chiral limit, leaving no adjustable free parameter in the present calculation. We compute the Sachs electric and magnetic form factors of the proton and neutron, the nucleon charge and magnetization radii, the magnetic moments, and the ratios $\mu_{p,n} G_E^{p,n}(Q^2)/G_M^{p,n}(Q^2)$. The present results are compared with the experimental data, the chiral quark-soliton model (χ QSM), and the Kelly parametrization. The proton charge radius, $\sqrt{\langle r_{\text{ch}}^2 \rangle^p} = 0.841$ fm, is in remarkable agreement with the recent muonic-hydrogen value, and the Q^2 dependence of the proton form-factor ratio $\mu_p G_E^p/G_M^p$ is reproduced very well, in clear contrast to the χ QSM. The overall agreement with the experimental data confirms that the effective chiral theory derived from the QCD instanton vacuum provides a consistent and predictive framework for describing the electromagnetic structure of the nucleon.

I. INTRODUCTION

Electromagnetic (EM) form factors are indispensable observables for unraveling the internal structure of the nucleon [1–3]. Since they encode the spatial distributions of the electric charge and magnetization, these form factors represent fundamental properties of the nucleon. The investigation of nucleon EM form factors has a long history, dating back to the pioneering electron-scattering experiments conducted by Hofstadter in the 1950s [4, 5]. The data on the neutron electric and magnetic form factors have been steadily refined over the decades [6–26]. The compilation of these data has enabled quantitative phenomenological fits [27–29]. In parallel, results from lattice calculations have also been refined [30–33]. Nevertheless, despite decades of extensive theoretical and experimental efforts, a complete understanding of these properties remains elusive, and several aspects are still subject to vigorous debate. A prominent example is the proton charge radius puzzle [34–47], in which discrepancies between recent precision measurements based on muonic and atomic hydrogen and the historical data from electron-proton scattering have revealed open questions in our understanding of the nucleon structure, calling for continued theoretical investigation (see also the following reviews [48–50]). The Particle Data Group (PDG) illustrates how the average value of the proton charge radius has evolved over the past two decades: in 2010, the PDG average was given as $\sqrt{\langle r_{\text{ch}}^2 \rangle^p} = 0.8768 \pm 0.0069$ fm [51], whereas it is now reported as $\sqrt{\langle r_{\text{ch}}^2 \rangle^p} = 0.8409 \pm 0.0004$ fm [52].

In the meantime, the EM structure of the nucleon has been examined from a more general perspective. The form factors of the nucleon are now regarded as the first moments of the generalized parton distributions (GPDs) [53–57]. The first moments of the vector GPDs are identified as the Dirac and Pauli form factors, which has also led to discussions of the transverse charge distributions of the nucleon, in which the significance of relativistic effects on the nucleon structure has been emphasized [58–60]. Moreover, the spin-orbit correlations in the nucleon are also deeply related to the EM form factors of the nucleon [61–63]. Considering that the spin-orbit correlations originate from the twist-3 effective spin-orbit correlation operator involving gluons, the EM structure of the nucleon may be connected to gluonic effects, even though gluons do not carry electric charge. Thus, precise information on the EM properties of the nucleon may shed light on the intricate internal quark-gluon structure of the nucleon.

In the present work, we therefore investigate the electromagnetic form factors of the nucleon and related observables on the basis of an effective chiral theory derived from the QCD instanton vacuum. The instanton dilute liquid model

* hjee6674@inha.edu

† sunctchoi@gmail.com

‡ hchkim@inha.ac.kr

was developed as a theoretical framework for explaining the nonperturbative structure of the QCD vacuum and the structure of low-lying hadrons [64–66] (see also the reviews [67, 68]). The instanton-antiinstanton medium is characterized by the average size of the instanton $\bar{\rho}$ and the average interdistance between instantons \bar{R} , which are approximately given by $\bar{\rho} \approx 1/3$ fm and $\bar{R} \approx 1$ fm when one uses $\Lambda_{\text{QCD}}^{\text{MS}} = 280$ MeV [64, 65, 68] (see also Ref. [69] for a detailed discussion of the instanton size). These values of $\bar{\rho}$ and \bar{R} yield the correct values of the gluon condensate [70] and of the topological susceptibility of the vacuum [71]. Since we consider a finite current quark mass, we need to reconstruct the instanton-antiinstanton medium beyond the chiral limit. In Refs. [72, 73], the saddle-point equation was derived in the presence of the $1/N_c$ meson-loop corrections and beyond the chiral limit, and the values of $\bar{\rho}$ and \bar{R} were readjusted to $\bar{\rho} = 0.35$ fm and $\bar{R} = 0.86$ fm, with $f_\pi = 88$ MeV and $\langle i\psi^\dagger\psi \rangle_0 = (255 \text{ MeV})^3$ required in the chiral limit. The present theoretical framework can be regarded as an effective theory for describing nonperturbative quark-gluon dynamics, characterized by the low-energy normalization point given by the inverse of the average instanton size, $\bar{\rho}^{-1} \approx 0.6$ GeV. We refer to Refs. [66, 71, 74, 75] for a detailed discussion.

The instanton vacuum naturally describes the spontaneous breakdown of chiral symmetry (SB χ S): as a quark propagates through the instanton-antiinstanton medium, it hops from one random instanton to an antiinstanton. Its helicity changes during this process, since the instanton zero mode has right-handed helicity whereas the antiinstanton zero mode has left-handed helicity. Repeating this process infinitely many times, the quark acquires a dynamical quark mass $M(k)$, which is momentum-dependent [66, 68]. The instanton vacuum then generates an effective nonlocal $2N_f$ quark-quark interaction, where N_f denotes the number of flavors. Bosonizing this quark-quark interaction, we obtain an effective chiral action with a momentum-dependent dynamical quark mass. The value of the dynamical quark mass at zero virtuality is determined by the saddle-point equation derived from the instanton vacuum [66, 68]. Once the value of Λ_{QCD} is given, all the dynamical parameters are fixed. Thus, we have no free parameters to adjust. Musakhanov improved the formalism of Diakonov and Petrov by incorporating the current quark mass beyond the chiral limit [76, 77].

The effective chiral theory of the nucleon that we employ for computing the nucleon EM form factors in this work is based on this effective nonlocal chiral action [78]. The local version of this effective chiral theory is known as the chiral quark-soliton model (χ QSM) [79–81] (see also the following reviews [82, 83]). This effective chiral theory of the nucleon was motivated by Witten’s pion mean-field idea [84–86]. In the pion mean-field picture, the nucleon can be viewed as a bound state of N_c (the number of colors) valence quarks in the large N_c limit. The presence of these valence quarks polarizes the vacuum self-consistently, and the vacuum polarization produces the pion mean field that binds the N_c valence quarks. This self-consistent interaction stabilizes the entire system consisting of the valence quarks and the Dirac continuum, and for this reason it has also been called a non-topological chiral soliton [82]. We will use this effective chiral theory as our theoretical framework to compute the EM form factors of the nucleon. Since the momentum-dependent dynamical quark mass plays the role of a regulator, we do not need to introduce any additional regularization to tame the divergences arising from quark loops. In addition, we also take into account the current quark mass [76, 77], since the isovector charge and magnetization radii of the nucleon diverge in the chiral limit [87].

This work is organized as follows. In Sec. II, we define the electromagnetic current and express its nucleon matrix element, which is parametrized in terms of the Dirac and Pauli form factors of the nucleon. We also relate these two form factors to the Sachs-type EM form factors. Section III explains the effective chiral theory of the nucleon based on the instanton vacuum. We recapitulate the formalism developed in Ref. [78]. We then show how the nucleon matrix element of the EM current can be computed within the present theoretical framework, and we derive the final expressions for the EM form factors of the nucleon. In Sec. IV, we present the numerical results for the EM form factors of the nucleon, and we compare them with the experimental data. We also compute the nucleon charge and magnetization radii, and present the results for the ratios of the electric and magnetic form factors. The final section is devoted to the summary and conclusions.

II. ELECTROMAGNETIC FORM FACTORS OF THE NUCLEON

The EM quark current in flavor SU(2) is defined as

$$J_\mu(x) = \bar{\psi}(x)\gamma_\mu\hat{Q}\psi(x), \quad (1)$$

where $\psi(x)$ denotes the quark field and γ_μ are the Dirac gamma matrices. \hat{Q} stands for the quark charge matrix, defined as

$$\hat{Q} = \begin{pmatrix} \frac{2}{3} & 0 \\ 0 & -\frac{1}{3} \end{pmatrix} = \frac{1}{6}\mathbf{1} + \frac{1}{2}\tau^3, \quad (2)$$

where τ^3 is the third component of the Pauli matrices. Accordingly, the EM current can be decomposed into the isoscalar and isovector vector currents:

$$J_\mu = J_\mu^{(0)} + J_\mu^{(3)}, \quad (3)$$

with

$$J_\mu^{(0)} = \frac{1}{6}\bar{\psi}(x)\gamma_\mu\psi(x), \quad J_\mu^{(3)} = \frac{1}{2}\bar{\psi}(x)\gamma_\mu\tau^3\psi(x). \quad (4)$$

The nucleon matrix element of the EM current can be parametrized in terms of two real EM form factors:

$$\begin{aligned} \langle N(p', S') | J_\mu(0) | N(p, S) \rangle &= \bar{u}_N(p', S') \left[\gamma_\mu F_1(Q^2) + \frac{i\sigma_{\mu\nu}\Delta^\nu}{2M_N} F_2(Q^2) \right] u_N(p, S) \\ &= \bar{u}_N(p', S') \left[\frac{M_N P^\mu}{P^2} G_E(Q^2) + \frac{i\epsilon^{\mu\nu\alpha\beta}\Delta_\nu P_\alpha \gamma_\beta \gamma_5}{2P^2} G_M(Q^2) \right] u_N(p, S), \end{aligned} \quad (5)$$

where M_N is the nucleon mass, $\Delta^\mu = (p' - p)^\mu$ is the spacelike four-momentum transfer, and $P^\mu = (p + p')^\mu / 2$ represents the average nucleon momentum. Q^2 is defined as the positive-definite momentum transfer squared, $Q^2 = -\Delta^2$ with $Q^2 > 0$. $u_N(p, S)$ denotes the Dirac spinor for the nucleon state with momentum p and spin S . $F_1(Q^2)$ and $F_2(Q^2)$ are called the Dirac and Pauli form factors, respectively, whereas $G_E(Q^2)$ and $G_M(Q^2)$ are known as the electric and magnetic Sachs form factors, respectively [88]. They are related to the Dirac and Pauli form factors as follows:

$$G_E(Q^2) = F_1(Q^2) - \frac{Q^2}{4M_N^2} F_2(Q^2), \quad (6)$$

$$G_M(Q^2) = F_1(Q^2) + F_2(Q^2). \quad (7)$$

The Sachs form factors $G_E(Q^2)$ and $G_M(Q^2)$ correspond to the temporal and spatial components of the nucleon matrix element, respectively, as follows:

$$\langle N(p', S') | J^0(0) | N(p, S) \rangle = \delta_{S'_3 S_3} G_E(Q^2), \quad (8)$$

$$\langle N(p', S') | J^i(0) | N(p, S) \rangle = \frac{i}{2M_N} \epsilon^{ijk} \langle \sigma^j \rangle_{S'_3 S_3} \Delta^k G_M(Q^2), \quad (9)$$

where $\langle \sigma^k \rangle_{S'_3 S_3}$ denotes the expectation value of the Pauli matrices with respect to the initial and final spin states of the nucleon. According to the definition of the isoscalar and isovector EM current given in Eq. (3), the Sachs form factors can be decomposed into the isoscalar and isovector ones,

$$G_{E(M)}^N(Q^2) = \frac{1}{2} \left(G_{E(M)}^{T=0}(Q^2) + \tau_3 G_{E(M)}^{T=1}(Q^2) \right), \quad (10)$$

where τ_3 corresponds to the eigenvalue for the third component of the isospin Pauli matrix. Thus, the proton and neutron electric form factors in the forward limit correspond to their charges

$$G_E^p(0) = 1, \quad G_E^n(0) = 0, \quad (11)$$

where the superscripts p and n denote the proton and neutron, respectively. The squared charge radii are defined as the slopes of the nucleon electric form factors at $Q^2 = 0$

$$\langle r^2 \rangle_E^{p(n)} = -6 \frac{dG_E^{p(n)}(Q^2)}{dQ^2} \Big|_{Q^2=0}. \quad (12)$$

Similarly, the proton and neutron magnetic form factors in the forward limit yield the corresponding magnetic moments,

$$\mu_{p(n)} = G_M^{p(n)}(0). \quad (13)$$

Finally, the squared magnetization radii are defined as follows:

$$\langle r^2 \rangle_M^{p(n)} = -\frac{6}{\mu_{p(n)}} \frac{dG_M^{p(n)}(Q^2)}{dQ^2} \Big|_{Q^2=0}. \quad (14)$$

In this work, we will compute the Sachs EM form factors of the nucleon within the framework of an effective chiral theory derived from the instanton vacuum.

III. EFFECTIVE CHIRAL THEORY FROM THE QCD INSTANTON VACUUM

We start from the effective low-energy QCD partition function obtained after bosonization of the $2N_f$ quark interactions [66, 68, 76, 77]:

$$\begin{aligned} \mathcal{Z}_{\text{eff}}[\psi^\dagger, \psi, \pi^a] = & \int \mathcal{D}\pi^a \int \mathcal{D}\psi^\dagger \mathcal{D}\psi \exp \left[\int d^4x \left\{ \psi_f^\dagger(x)(i\cancel{\partial})\psi_f(x) + i\psi_f^\dagger(x)m_f\psi_f(x) \right. \right. \\ & \left. \left. + iM_0f(m_f) \int \frac{d^4k d^4l}{(2\pi)^8} e^{i(k-l)\cdot x} F(k)F(l)\psi_f^\dagger(k) (U_g^f(x)P_L + U_g^{\dagger f}(x)P_R) \psi_f(l) \right\} \right], \end{aligned} \quad (15)$$

where π^a represent the pseudo-Nambu-Goldstone (pNG) boson fields, $\psi_f(x)$ is the quark field with flavor f , and m_f denotes the current quark mass with flavor f . We assume isospin symmetry ($m_u = m_d$), and we define the average current quark mass of the up and down quarks as $\bar{m} = (m_u + m_d)/2$. The quark form factor $F(k)$ arises from the Fourier transform of the fermionic zero mode in the instanton background field:

$$F(k) = -z \frac{d}{dz} \left[I_0(z)K_0(z) - I_1(z)K_1(z) \right] \Big|_{z=\frac{\bar{\rho}k}{2}}, \quad (16)$$

where $I_n(x)$ and $K_n(x)$ denote the modified Bessel functions of the first and second kinds, respectively. Owing to this form factor, the dynamical quark mass $M(k)$ becomes momentum-dependent. The function $f(m_f)$ originates from the m_f dependence of the dynamical quark mass [77]:

$$f(m_f) = \sqrt{1 + \frac{m_f^2}{d^2} - \frac{m_f}{d}}, \quad (17)$$

where $d \approx 277$ MeV. Note that d is naturally determined once the values of $\bar{\rho}$ and \bar{R} are known. The chiral field $U(x)$ is defined as $U(x) := \exp[i\pi^a(x)\tau^a]$ with $a = 1, 2, 3$. P_L and P_R stand for the left-handed and right-handed chirality projection operators, expressed as $P_L = (1 - \gamma_5)/2$ and $P_R = (1 + \gamma_5)/2$, respectively. The combination $U(x)P_L + U^\dagger(x)P_R$ can be written in the following compact form:

$$U^{\gamma_5}(x) := \exp(i\pi^a \tau^a \gamma_5) = U(x)P_L + U^\dagger(x)P_R. \quad (18)$$

Integrating over the quark fields, we obtain the following effective partition function:

$$\mathcal{Z}_{\text{eff}}[\pi^a] = \int \mathcal{D}\pi^a \text{Det} \left[i\cancel{\partial} + i\bar{m}\mathbf{1} + iM_0f(\bar{m})\overleftarrow{F}(i\partial)U^{\gamma_5}[\pi^a(x)]\overrightarrow{F}(i\partial) \right]. \quad (19)$$

In the large N_c limit, the pionic quantum fluctuations are suppressed by $1/N_c$. Thus, we can integrate over the π^a fields in Eq. (19) around the classical saddle point [84–86], which yields the nonlocal effective chiral action (NE χ A)

$$S_{\text{eff}}[U] = -N_c \text{Tr} \log(D[U]), \quad (20)$$

where the Dirac differential operator $D[U]$ is given by

$$D[U] = i\cancel{\partial} + i\bar{m} + iM_0f(\bar{m})\overleftarrow{F}(i\partial)U^{\gamma_5}(x)\overrightarrow{F}(i\partial). \quad (21)$$

$H[U]$ is the single-particle Dirac Hamiltonian written as

$$H[U] = \gamma_4 \gamma_i \partial_i + \gamma_4 \bar{m} + M_0 f(\bar{m}) \overleftarrow{F} \gamma_4 U^{\gamma_5} \overrightarrow{F}. \quad (22)$$

In the present mean-field approach, the nucleon consists of N_c valence quarks [79, 82, 83], which are described by the quark propagator in the background pion field [78]

$$G_{f_i g_i}(\mathbf{0}, +\mathcal{T}/2 | \mathbf{0}, -\mathcal{T}/2) = \langle \mathbf{0}, +\mathcal{T}/2, f_i | D[U]^{-1} i\gamma_4 | \mathbf{0}, -\mathcal{T}/2, g_i \rangle = \int \frac{d\omega}{2\pi} \left\langle \mathbf{0}, f_i \left| \frac{1}{-i\omega + H} \right| \mathbf{0}, g_i \right\rangle e^{-i\omega\mathcal{T}}, \quad (23)$$

where the single-particle Dirac Hamiltonian can be diagonalized as $H|n_\omega\rangle = E_n(\omega)|n_\omega\rangle$. Note that the eigenenergies are given as functions of ω . The detailed formalism for constructing the classical nucleon within this effective chiral theory can be found in Ref. [78].

To investigate the EM form factors of the nucleon within the present effective chiral theory, we have to introduce the EM current into the low-energy effective QCD partition function in Eq. (15). However, the nonlocal interaction arising from the momentum-dependent quark mass breaks the U(1) gauge symmetry [89]. Many efforts have been devoted to resolving this problem [89–97]. As pointed out by Pobylytsa [98], the breakdown of the gauge symmetry in the QCD instanton vacuum is deeply rooted in the treatment of higher-order contributions to hadronic correlation functions in the N/VN_c expansion, where N/V denotes the density of the instanton medium. However, it is technically formidable to deal with such higher-order corrections. Musakhanov and Kim [99] introduced the external EM field into the QCD action and kept the gauge invariance intact by introducing the gauge connection in the course of constructing the effective $2N_f$ quark interactions. In the weak photon field, it was shown that the gauge invariance can be preserved by replacing the ordinary derivative with the covariant one [99], which is identical to the well-known minimal substitution. This method has been successfully applied to many observables [73, 100–106]. In Ref. [78], the conservation of the baryon number was demonstrated using this method. Following Ref. [99], we can express the gauged effective low-energy partition function as

$$Z_{\text{eff}}[\pi^a, v] = \int \mathcal{D}\pi^a \exp(-S_{\text{eff}}[\pi^a, v]), \quad (24)$$

where the gauged NE χ A is given by

$$S_{\text{eff}}[U, v] = -N_c \text{Tr} \log [D(U, v)] \quad (25)$$

with

$$D(U, v) = i\nabla\!\!\!/ + i\overline{m} + iM_0 \overleftarrow{F}(i\nabla)U\gamma_5(x)\overrightarrow{F}(i\nabla). \quad (26)$$

Here, ∇ denotes the covariant derivative

$$\nabla_\mu = \partial_\mu - i\mathcal{V}_\mu, \quad (27)$$

where \mathcal{V}_μ is the external photon field defined as $\mathcal{V}_\mu = \hat{Q}v_\mu$.

To compute a nucleon matrix element in the present work, we have to define the nucleon state. In the effective chiral theory, the nucleon state consists of N_c valence quarks, which can be expressed as

$$\begin{aligned} |N(p, S)\rangle &= \mathcal{N}^*(p) \lim_{x_4 \rightarrow -\infty} e^{ip_4 x_4} \int d^3x e^{i\mathbf{p}\cdot\mathbf{x}} J_N^\dagger(x) |0\rangle, \\ \langle N(p', S')| &= \mathcal{N}(p') \lim_{y_4 \rightarrow +\infty} e^{-ip'_4 y_4} \int d^3y e^{-i\mathbf{p}'\cdot\mathbf{y}} \langle 0| J_N(y), \end{aligned} \quad (28)$$

where \mathcal{N}^* and \mathcal{N} are the normalization constants of the nucleon state. The Ioffe-type current J_N consisting of N_c quark fields is defined as

$$J_N(x) = \frac{1}{N_c!} \varepsilon^{\alpha_1 \dots \alpha_{N_c}} \Gamma_{(TT_3)(SS_3)}^{f_1 \dots f_{N_c}} \psi_{\alpha_1 f_1}(x) \dots \psi_{\alpha_{N_c} f_{N_c}}(x), \quad (29)$$

where α and β denote color indices, f and g denote flavor indices, and Γ represents the matrices carrying the flavor and spin quantum numbers TT_3 and SS_3 of the nucleon. As mentioned in Sec. II, the EM form factors of the nucleon are defined through the matrix element of the EM current given in Eq. (5). This nucleon matrix element can be expressed as the following three-point correlation function in Euclidean space:

$$\begin{aligned} \langle N(p', S') | J_\mu(0) | N(p, S) \rangle &= \mathcal{N}^*(p') \mathcal{N}(p) \lim_{\substack{y_4 \rightarrow +\infty \\ x_4 \rightarrow -\infty}} e^{-ip'_4 y_4 + ip_4 x_4} \int d^3y d^3x e^{-i\mathbf{p}'\cdot\mathbf{y} + i\mathbf{p}\cdot\mathbf{x}} \\ &\quad \times \langle 0 | J_N(y) (-i) \psi^\dagger \hat{Q} \gamma_\mu \psi J_N^\dagger(x) | 0 \rangle. \end{aligned} \quad (30)$$

In the large Euclidean-time limit, the three-point correlation function can be written as

$$\langle 0 | J_N(y) (-i) \psi^\dagger \hat{Q} \gamma_\mu \psi J_N^\dagger(x) | 0 \rangle = \frac{1}{\mathcal{Z}_{\text{eff}}[0]} \int \mathcal{D}U \mathcal{D}\psi^\dagger \mathcal{D}\psi \exp \left[\int d^4x \psi_f^\dagger(x) D(U, v) \psi^f(x) \right]. \quad (31)$$

To evaluate the three-point correlation function in Eq. (31), we introduce the following generating functional in Euclidean space:

$$\begin{aligned} \mathcal{W}[\eta^\dagger, \eta, v] &= \frac{-i}{\mathcal{Z}_{\text{eff}}[0]} \int \mathcal{D}\psi^\dagger \mathcal{D}\psi \mathcal{D}U \exp \left[\int d^4x \left\{ \psi^\dagger(x) (i\nabla + i\bar{m}\mathbf{1}) \psi(x) - i\eta^\dagger(x) \psi(x) - i\psi^\dagger(x) \eta(x) \right. \right. \\ &\quad \left. \left. + iM_0 f(\bar{m}) \int \frac{d^4k d^4l}{(2\pi)^8} e^{i(k-l)\cdot x} F(k + \hat{Q}v) F(l + \hat{Q}v) \psi^\dagger(k) U^{\gamma_5}(x) \psi(l) \right\} \right] \\ &= \frac{-i}{\mathcal{Z}_{\text{eff}}[0]} \int \mathcal{D}U \text{Det} [D(U, v)] \exp \left[- \int d^4x d^4y \eta^\dagger(x) \left\langle x \left| \frac{1}{D(U, v)} \right| y \right\rangle \eta(y) \right], \end{aligned} \quad (32)$$

where η denotes the source field for the fermion. The three-point correlation function in Eq. (31) can then be computed explicitly by taking the functional derivatives of the generating functional:

$$\begin{aligned} \langle 0 | J_N(y) (-i) \psi^\dagger(0) \hat{Q} \gamma_\mu \psi(0) J_N^\dagger(x) | 0 \rangle &= \Gamma_{(TT'_3)(SS'_3)}^{\{f\}} (\Gamma_{(TT_3)(SS_3)}^{\{g\}})^* \frac{\delta}{\delta \eta_{f_1}^\dagger(\mathbf{y}, y_4)} \cdots \frac{\delta}{\delta \eta_{f_{N_c}}^\dagger(\mathbf{y}, y_4)} \frac{\delta}{\delta v_\mu(0)} \\ &\quad \times \mathcal{W}[\eta^\dagger, \eta, v] \Big|_{\eta^\dagger, \eta, v=0} \frac{\overleftarrow{\delta}}{\delta \eta_{g_1}(\mathbf{x}, x_4)} \cdots \frac{\overleftarrow{\delta}}{\delta \eta_{g_{N_c}}(\mathbf{x}, x_4)}. \end{aligned} \quad (33)$$

The result for the EM matrix element can be decomposed into the valence (level-quark) and sea (Dirac-continuum) contributions:

$$\langle N(p', S') | J_\mu(0) | N(p, S) \rangle = \langle N(p', S') | J_\mu(0) | N(p, S) \rangle_{\text{val}} + \langle N(p', S') | J_\mu(0) | N(p, S) \rangle_{\text{sea}}, \quad (34)$$

where the valence contribution is given by

$$\begin{aligned} \langle N(p', S') | J_\mu(0) | N(p, S) \rangle_{\text{val}} &= \frac{N_c}{\mathcal{Z}_{\text{eff}}[0]} \Gamma_{(TT'_3)(SS'_3)}^{\{f\}} (\Gamma_{(TT_3)(SS_3)}^{\{g\}})^* \\ &\quad \times \lim_{T \rightarrow \infty} e^{-i(p'_4 + p_4) \frac{T}{2}} \int d^3x d^3y e^{-i\mathbf{p}' \cdot \mathbf{y} + i\mathbf{p} \cdot \mathbf{x}} \int \mathcal{D}U e^{-S_{\text{eff}}[U]} \prod_{i=2}^{N_c} \left\langle \mathbf{y}, \frac{T}{2} \left| \frac{1}{D[U]} \right| \mathbf{x}, -\frac{T}{2} \right\rangle_{f_i, g_i} \\ &\quad \times \left\langle \mathbf{y}, \frac{T}{2} \left| \frac{1}{D[U]} \right| \mathbf{0}, 0 \right\rangle_{f_1, f} \left\{ i\gamma_4 \gamma_\mu \hat{Q} - \gamma_4 M_0 f(\bar{m}) (\overleftarrow{F}_\mu \hat{Q} U^{\gamma_5} \overrightarrow{F} + \overleftarrow{F} U^{\gamma_5} \hat{Q} \overrightarrow{F}_\mu) \right\}_{fg} \left\langle \mathbf{0}, 0 \left| \frac{1}{D[U]} \right| \mathbf{x}, -\frac{T}{2} \right\rangle_{g, g_1}, \end{aligned} \quad (35)$$

whereas the sea contribution is given by

$$\begin{aligned} \langle N(p', S') | J_\mu(0) | N(p, S) \rangle_{\text{sea}} &= \frac{N_c}{\mathcal{Z}_{\text{eff}}[0]} \Gamma_{(TT'_3)(SS'_3)}^{\{f\}} (\Gamma_{(TT_3)(SS_3)}^{\{g\}})^* \\ &\quad \times \lim_{T \rightarrow \infty} e^{-i(p'_4 + p_4) \frac{T}{2}} \int d^3x d^3y e^{-i\mathbf{p}' \cdot \mathbf{y} + i\mathbf{p} \cdot \mathbf{x}} \int \mathcal{D}U e^{-S_{\text{eff}}[U]} \prod_{i=1}^{N_c} \left\langle \mathbf{y}, \frac{T}{2} \left| \frac{1}{D[U]} \right| \mathbf{x}, -\frac{T}{2} \right\rangle_{f_i, g_i} \\ &\quad \times \text{tr} \left[\left\{ i\gamma_4 \gamma_\mu \hat{Q} - \gamma_4 M_0 f(\bar{m}) (\overleftarrow{F}_\mu \hat{Q} U^{\gamma_5} \overrightarrow{F} + \overleftarrow{F} U^{\gamma_5} \hat{Q} \overrightarrow{F}_\mu) \right\} \left\langle \mathbf{0}, 0 \left| \frac{1}{D[U]} \right| \mathbf{0}, 0 \right\rangle \right]. \end{aligned} \quad (36)$$

where $F_\mu = \partial F / \partial k_\mu$ is defined as the derivative of $F(k)$ with respect to k_μ . As mentioned above, the path integral over the chiral field U is performed within the saddle-point approximation. However, the translational and rotational zero modes must be treated exactly. Explicitly, these zero modes can be incorporated as

$$U_c(\mathbf{r}) \longrightarrow R(t) T(\mathbf{Z}(t)) U_c(\mathbf{r}) T^\dagger(\mathbf{Z}(t)) R^\dagger(t) = R(t) U(\mathbf{r} - \mathbf{Z}(t)) R^\dagger(t), \quad (37)$$

where the rotational matrix R is an element of the SU(2) group. The translational operator $T(\mathbf{Z}(t))$ shifts the position of the mean field to $\mathbf{r} - \mathbf{Z}(t)$. Note that the translational zero modes naturally yield the Fourier transform of the three-dimensional charge and magnetization distributions.

The path integration over the U field, $\mathcal{D}U$, is then replaced by integration over the zero modes [82]

$$\int \mathcal{D}U \mathcal{F}[U(x)] \rightarrow \int \mathcal{D}R \mathcal{D}\mathbf{Z} \mathcal{F}[TRU_c(\mathbf{r}) R^\dagger T^\dagger]. \quad (38)$$

The Dirac operator given in Eq. (21) can be rewritten as

$$D[U] = R(t)T(\mathbf{Z}(t))i\gamma_4 \left[D[U_c] + \frac{i}{2}\Omega^a t^a \right] T^\dagger(\mathbf{Z}(t))R^\dagger(t), \quad (39)$$

where $D[U_c] = \partial_4 + H[U_c]$ and Ω^a is the angular velocity defined by

$$R^\dagger \dot{R} = i\Omega = \frac{i}{2}\Omega^a \tau^a. \quad (40)$$

Note that t^a in Eq. (39) contains both local and nonlocal contributions:

$$t^a = \tau^a + i\gamma_4 M_0 f(\bar{m}) \left(\overleftarrow{F}_4 \tau^a U_c^{\gamma_5} \overrightarrow{F} + \overleftarrow{F} U_c^{\gamma_5} \tau^a \overrightarrow{F}_4 \right), \quad (41)$$

where the second term arises from the momentum-dependent dynamical quark mass.

Having performed the calculation of the $1/N_c$ rotational corrections [78, 82, 107, 108], we arrive at the final expressions for the EM Sachs form factors of the nucleon. The isoscalar electric form factor receives contributions only from the leading order in the N_c expansion:

$$G_E^{T=0}(Q^2) = \frac{N_c}{3} \int d^3r j_0(|\mathbf{Q}||\mathbf{r}|) \mathcal{B}(\mathbf{r}), \quad (42)$$

where $\mathcal{B}(\mathbf{r})$ is identified as the baryonic density expressed as

$$\begin{aligned} \mathcal{B}(\mathbf{r}) &= z_{\text{val}} \langle \text{val} | \mathbf{r} \rangle \left\{ 1 + i\gamma_4 M_0 f(\bar{m}) \left(\overleftarrow{F}_4 U_c^{\gamma_5} \overrightarrow{F} + \overleftarrow{F} U_c^{\gamma_5} \overrightarrow{F}_4 \right) \right\} \langle \mathbf{r} | \text{val} \rangle \\ &+ \int \frac{d\omega}{2\pi i} \sum_n \frac{\langle n_\omega | \mathbf{r} \rangle \left\{ 1 + i\gamma_4 M_0 f(\bar{m}) \left(\overleftarrow{F}_4 U_c^{\gamma_5} \overrightarrow{F} + \overleftarrow{F} U_c^{\gamma_5} \overrightarrow{F}_4 \right) \right\} \langle \mathbf{r} | n_\omega \rangle}{\omega + iE_n(\omega)}. \end{aligned} \quad (43)$$

The first term of Eq. (43) comes from the valence-quark contribution, whereas the second one comes from the sea-quark contribution. To obtain the isovector electric form factor, we have to take into account the $1/N_c$ rotational corrections:

$$G_E^{T=1}(Q^2) = \frac{1}{I} \int d^3r j_0(|\mathbf{Q}||\mathbf{r}|) \mathcal{I}(\mathbf{r}), \quad (44)$$

where $\mathcal{I}(\mathbf{r})$ denotes the density of the moment of inertia, given by

$$\begin{aligned} \mathcal{I}(\mathbf{r}) &= \frac{N_c}{6} \left(z_{\text{val}} \sum_n \frac{\langle \text{val} | \mathbf{r} \rangle t^a \langle \mathbf{r} | n_{\omega_v} \rangle \langle n_{\omega_v} | t^a | \text{val} \rangle}{E_n(\omega_v) - E_{\text{val}}} + \frac{1}{2} z_{\text{val}} \langle \text{val} | \mathbf{r} \rangle T^{aa} \langle \mathbf{r} | \text{val} \rangle \right. \\ &\left. + \frac{1}{2} \int \frac{d\omega}{2\pi} \sum_{n,m} \frac{\langle m_\omega | \mathbf{r} \rangle t^a \langle \mathbf{r} | n_\omega \rangle \langle n_\omega | t^a | m_\omega \rangle}{[\omega + iE_n(\omega)][\omega + iE_m(\omega)]} + \frac{1}{2} \int \frac{d\omega}{2\pi i} \sum_n \frac{\langle n_\omega | \mathbf{r} \rangle T^{aa} \langle \mathbf{r} | n_\omega \rangle}{\omega + iE_n(\omega)} \right). \end{aligned} \quad (45)$$

where $\omega_v = -iE_{\text{val}}(\omega_v)$. A detailed discussion for this quantity is in Ref. [109]. The operators t^a and T^{ab} in isospin space in Eq. (45) are defined as

$$t^a = \tau^a + i\gamma_4 M_0 f(\bar{m}) \left(\overleftarrow{F}_4 \tau^a U_c^{\gamma_5} \overrightarrow{F} + \overleftarrow{F} U_c^{\gamma_5} \tau^a \overrightarrow{F}_4 \right), \quad (46)$$

$$T^{ab} = \gamma_4 M_0 f(\bar{m}) \left(\overleftarrow{F}_{44} \tau^a \tau^b U_c^{\gamma_5} \overrightarrow{F} + 2\overleftarrow{F}_4 \tau^a U_c^{\gamma_5} \tau^b \overrightarrow{F}_4 + \overleftarrow{F} U_c^{\gamma_5} \tau^a \tau^b \overrightarrow{F}_{44} \right). \quad (47)$$

The valence and sea contributions to the moment of inertia are given by¹

$$\begin{aligned} I_{\text{val}} \delta^{ab} &= \frac{N_c}{2} z_{\text{val}} \sum_n \frac{\langle \text{val} | t^a | n_{\omega_v} \rangle \langle n_{\omega_v} | t^b | \text{val} \rangle}{E_n(\omega_v) - E_{\text{val}}} + \frac{N_c}{4} z_{\text{val}} \langle \text{val} | T^{ab} | \text{val} \rangle, \\ I_{\text{sea}} \delta^{ab} &= \frac{N_c}{4} \sum_{n,m} \int \frac{d\omega}{2\pi} \frac{\langle m_\omega | t^a | n_\omega \rangle \langle n_\omega | t^b | m_\omega \rangle}{\omega + iE_n(\omega) \omega + iE_m(\omega)} + \frac{N_c}{4} \sum_n \int \frac{d\omega}{2\pi i} \frac{\langle n_\omega | T^{ab} | n_\omega \rangle}{\omega + iE_n(\omega)}. \end{aligned} \quad (48)$$

¹ The expressions for the moment of inertia in Ref. [78] contain typographical errors, which are corrected in the present work.

If we switch off the momentum dependence of the dynamical quark mass, the results for the electric form factors of the nucleon reduce to those in the χ QSM [82, 107] without regularization.

The isoscalar magnetic form factor again arises from the next-to-leading-order contribution in the $1/N_c$ expansion:

$$G_M^{T=0}(Q^2) = \frac{N_c M_N}{4I} \int d^3r \frac{j_1(|\mathbf{Q}||\mathbf{r}|)}{|\mathbf{Q}||\mathbf{r}|} \mathcal{X}(\mathbf{r}), \quad (49)$$

where the density $\mathcal{X}(\mathbf{r})$ is given by

$$\begin{aligned} \mathcal{X}(\mathbf{r}) &= 2z_{\text{val}} \sum_n \frac{\langle \text{val}|\mathbf{r}\rangle t_{M,T=0}^{zz} \langle \mathbf{r}|n_\omega\rangle \langle n_\omega|t^z|\text{val}\rangle}{E_n(\omega) - E_{\text{val}}} + z_{\text{val}} \langle \text{val}|\mathbf{r}\rangle iT_{M,T=0}^{zz} \langle \mathbf{r}|\text{val}\rangle \\ &+ \int \frac{d\omega}{2\pi} \sum_{n,m} \frac{\langle m_\omega|\mathbf{r}\rangle t_{M,T=0}^{zz} \langle \mathbf{r}|n_\omega\rangle \langle n_\omega|t^z|m_\omega\rangle}{[\omega + iE_n(\omega)][\omega + iE_m(\omega)]} + \int \frac{d\omega}{2\pi i} \sum_n \frac{\langle n_\omega|\mathbf{r}\rangle iT_{M,T=0}^{zz} \langle \mathbf{r}|n_\omega\rangle}{\omega + iE_n(\omega)}. \end{aligned} \quad (50)$$

$t_{M,T=0}^i$ and $T_{M,T=0}^{ia}$ are defined respectively as

$$t_{M,T=0}^i = -\gamma_5(\mathbf{r} \times \boldsymbol{\sigma})_i - \gamma_4 M_0 f(\bar{m}) \left(\overleftarrow{F}' L_i U_c \gamma_5 \overrightarrow{F} + \overleftarrow{F} U_c \gamma_5 L_i \overrightarrow{F}' \right) \quad (51)$$

and

$$T_{M,T=0}^{ia} = \gamma_4 M_0 f(\bar{m}) \left(\overleftarrow{F}'_4 L_i \tau^a U_c \gamma_5 \overrightarrow{F} + \overleftarrow{F}' L_i U_c \gamma_5 \tau^a \overrightarrow{F}'_4 + \overleftarrow{F}'_4 \tau^a U_c \gamma_5 L_i \overrightarrow{F}' + \overleftarrow{F} U_c \gamma_5 \tau^a L_i \overrightarrow{F}'_4 \right), \quad (52)$$

where $F' = \partial F / \partial k^2$ is defined as the derivative of $F(k)$ with respect to k^2 and L_i is the orbital angular momentum operator. The isovector magnetic form factor contains both the leading-order and $1/N_c$ -order contributions:

$$G_M^{T=1}(Q^2) = N_c M_N \int d^3r \frac{j_1(|\mathbf{Q}||\mathbf{r}|)}{|\mathbf{Q}||\mathbf{r}|} \left(\mathcal{Q}_0(\mathbf{r}) - \frac{1}{4I} \mathcal{Q}_1(\mathbf{r}) \right), \quad (53)$$

where $\mathcal{Q}_0(\mathbf{r})$ and $\mathcal{Q}_1(\mathbf{r})$ are given by

$$\mathcal{Q}_0(\mathbf{r}) = z_{\text{val}} \langle \text{val}|\mathbf{r}\rangle t_{M,T=1}^{zz} \langle \mathbf{r}|\text{val}\rangle + \int \frac{d\omega}{2\pi i} \sum_n \frac{\langle n_\omega|\mathbf{r}\rangle t_{M,T=1}^{zz} \langle \mathbf{r}|n_\omega\rangle}{\omega + iE_n(\omega)} \quad (54)$$

and

$$\begin{aligned} \mathcal{Q}_1(\mathbf{r}) &= i\epsilon_{zij} \left[2z_{\text{val}} \sum_n z_n \text{sign}(E_n) \frac{\langle \text{val}|\mathbf{r}\rangle t_{M,T=1}^{zj} \langle \mathbf{r}|n_{\omega_n}\rangle \langle n_{\omega_n}|t^i|\text{val}\rangle}{E_n(\omega_n) - E_{\text{val}}(\omega_v)} + z_{\text{val}} \langle \text{val}|\mathbf{r}\rangle iT_{M,T=1}^{zij} \langle \mathbf{r}|\text{val}\rangle \right. \\ &+ \int \frac{d\omega_1}{2\pi} \frac{d\omega_2}{2\pi} \mathcal{P} \left(\frac{2i}{\omega_2 - \omega_1} \right) \sum_{n,m} \frac{\langle m_{\omega_1}|\mathbf{r}\rangle t_{M,T=1}^{zj} \langle \mathbf{r}|n_{\omega_2}\rangle \langle n_{\omega_2}|t^i|m_{\omega_1}\rangle}{[\omega_1 + iE_m(\omega_1)][\omega_2 + iE_n(\omega_2)]} \\ &\left. + \int \frac{d\omega}{2\pi i} \sum_{n_\omega} \frac{\langle n_\omega|\mathbf{r}\rangle iT_{M,T=1}^{zij} \langle \mathbf{r}|n_\omega\rangle}{\omega + iE_n(\omega)} \right], \end{aligned} \quad (55)$$

where $\omega_n = -iE_n(\omega_n)$ and \mathcal{P} stands for the Cauchy principal value. The operators $t_{M,T=1}^{ia}$ and $T_{M,T=1}^{iab}$ are defined respectively as

$$t_{M,T=1}^{ia} = -\gamma_5(\mathbf{r} \times \boldsymbol{\sigma})_i \tau^a - \gamma_4 M_0 f(\bar{m}) \left(\overleftarrow{F}' L_i \tau^a U_c \gamma_5 \overrightarrow{F} + \overleftarrow{F} U_c \gamma_5 \tau^a L_i \overrightarrow{F}' \right) \quad (56)$$

and

$$T_{M,T=1}^{iab} = \gamma_4 M_0 f(\bar{m}) \left(-\overleftarrow{F}'_4 L_i \tau^a \tau^b U_c \gamma_5 \overrightarrow{F} + \overleftarrow{F}' L_i \tau^b U_c \gamma_5 \tau^a \overrightarrow{F}'_4 - \overleftarrow{F}'_4 \tau^a U_c \gamma_5 \tau^b L_i \overrightarrow{F}' + \overleftarrow{F} U_c \gamma_5 \tau^b \tau^a L_i \overrightarrow{F}'_4 \right). \quad (57)$$

Once again, the results for the magnetic form factors of the nucleon become identical to the nonregularized expressions of the χ QSM [82, 107] when the momentum dependence of the dynamical quark mass is switched off.

IV. RESULTS AND DISCUSSION

Since we start from the improved effective low-energy QCD partition function given in Eq. (15) beyond the chiral limit, the average size of the instanton and the average interdistance between instantons are fixed to $\bar{\rho} = 0.35$ fm and $\bar{R} = 0.86$ fm, respectively. In addition, we take the average value of the current up- and down-quark masses to be $\bar{m} = 5$ MeV [110], which yields the pion mass $m_\pi = 140$ MeV. The dynamical quark mass at zero virtuality is determined to be $M_0 = 385$ MeV from the saddle-point equation beyond the chiral limit [73, 110]. Thus, we have no adjustable free parameter in the present calculation. In Ref. [78], the effective chiral theory based on the instanton vacuum was developed in the chiral limit. Therefore, we need to compute the classical nucleon mass and the moment of inertia with the current quark mass taken into account. The momentum-dependent quark mass in the valence-quark part gives rise to fundamental complications related to the analytic continuation from Euclidean to Minkowski space, since the momentum-dependent dynamical quark mass derived from the instanton vacuum is strictly defined in Euclidean space. For this reason, we retain the momentum dependence of the dynamical quark mass only in the sea-quark (Dirac-continuum) part. This approximation is nevertheless justified, since the valence part is finite and thus does not require any regularization. For the same reason, the valence part was also not regularized in the χ QSM. Finally, we want to mention that the momentum-dependent dynamical quark mass requires a much larger box size than that in the χ QSM in order to ensure numerical stability. We use a box size of $D_{\text{box}} \approx 11$ fm. Note that we solve the single-particle Dirac equation by using the Kahana-Ripka method [111].

TABLE I. Classical nucleon mass M_{cl} . The second row presents the results of the present work, whereas the third row corresponds to those obtained in the chiral limit. The fourth and fifth rows show the results obtained in the χ QSM with the dynamical quark mass $M_0 = 385$ MeV and $M_0 = 420$ MeV, respectively.

	E_{val} [MeV]	$N_c E_{\text{val}}$ [MeV]	E_{sea} [MeV]	M_{cl} [MeV]
This work ($M_0=385$ MeV)	162.2	486.5	530.1	1017
Chiral limit($M_0=359$ MeV)	152.6	457.7	529.7	987.4
χ QSM($M_0=385$ MeV)	223.3	669.8	588.0	1258
χ QSM($M_0=420$ MeV)	203.5	610.6	645.8	1256

The classical nucleon mass [79] is expressed as

$$M_{\text{cl}} = \min_{\pi(x)} [N_c E_{\text{val}} + E_{\text{sea}}], \quad (58)$$

where E_{val} and E_{sea} stand for the valence-quark and sea-quark energies, respectively. The saddle-point approximation, which we apply to the integration over the chiral field, gives rise to the equation of motion for the classical pion field. Its solution defines the pion mean field and is determined through a self-consistent iterative procedure. Details of the minimization scheme for M_{cl} can be found in Refs. [78, 82]. Table I summarizes the present numerical results for the classical nucleon mass together with those obtained within the χ QSM. Since the current quark mass is incorporated here, we further compare our values with the corresponding ones in the chiral limit. For the chiral-limit case, we follow Ref. [66], in which the instanton parameters are fixed to $\bar{\rho} = 1/3$ fm and $\bar{R} = 1$ fm, while the dynamical quark mass at zero virtuality is determined to be $M_0 = 359$ MeV. As seen by comparing the second and third rows, the current quark mass mainly influences the valence-quark part, leaving the sea-quark part nearly unchanged.

In the fourth and fifth rows, we list the results from the χ QSM with the values of the dynamical quark mass $M_0 = 385$ MeV and 420 MeV, respectively. In the χ QSM, $M_0 = 420$ MeV is selected, because it yields the best results for baryonic observables in comparison with experimental data. However, the constant M inevitably requires a regularization scheme to tame quark loops. For the present comparison, we adopt the proper-time regularization, in which the cutoff mass Λ is fixed so as to reproduce the experimental value of the pion decay constant f_π . A single cutoff, however, leads to a current quark mass of $m_u = m_d \approx 15$ MeV when the pion mass is constrained to $m_\pi = 140$ MeV [81]. Compared with the results from the χ QSM, the present ones are consistently smaller. As a result, the value of the classical nucleon mass turns out to be closer to the experimental value of the nucleon mass.

In Table II, we list the numerical results for the moment of inertia, which is defined in Eq. (48), which are also compared with those from the χ QSM. Comparing the results in the second row with those in the third row, we observe that the introduction of the current quark mass suppresses the sea-quark contribution to the moment of inertia. The

TABLE II. Moments of inertia in units of fm. The second row presents the results of the present work, whereas the third row corresponds to those obtained in the chiral limit. The fourth and fifth rows show the results obtained in the χ QSM with the dynamical quark mass $M_0 = 385$ MeV and $M_0 = 420$ MeV, respectively. In the last column, the results for the Δ - N mass splitting are given in units of MeV.

	I_{val} [fm]	I_{sea} [fm]	I [fm]	$M_{\Delta-N}$ [MeV]
This work ($M_0=385$ MeV)	1.075	0.089	1.164	254.2
Chiral limit($M_0=359$ MeV)	1.085	0.315	1.400	211.5
χ QSM($M_0=385$ MeV)	0.949	0.248	1.197	247.3
χ QSM($M_0=420$ MeV)	0.775	0.255	1.031	287.2

value of I directly determines the $\Delta - N$ mass difference [78, 79, 112], which is given by

$$M_{\Delta-N} = M_{\Delta} - M_N = \frac{3}{2I}. \quad (59)$$

This work yields $M_{\Delta-N} = 254.2$ MeV, which is closer to the experimental center value of the Δ isobar, $(M_{\Delta} - M_N)_{\text{Exp}} \approx (270 - 290)$ MeV [52].

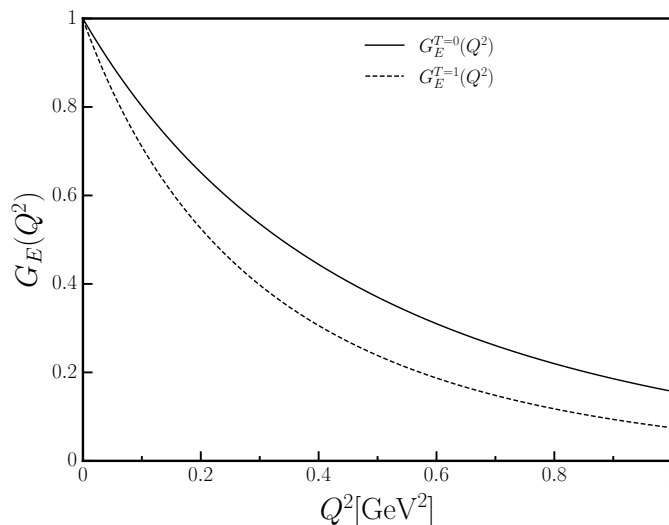


FIG. 1. Isoscalar and isovector electric form factors of the nucleon. The solid curve represents the result for the isoscalar electric form factor, whereas the dashed one denotes that for the isovector electric form factor.

In Fig. 1, the numerical results for the isoscalar and isovector electric form factors are shown. As given in Eq. (42), $G_E^{T=0}(Q^2)$ arises from the baryon density, whereas $G_E^{T=1}(Q^2)$, given in Eq. (44), originates from the $1/N_c$ rotational corrections. Thus, the contribution from the baryon density is of leading order in the large N_c expansion. As expected from this N_c counting, the isoscalar electric form factor is larger than the isovector one over the entire Q^2 range considered.

In Fig. 2, we draw the numerical result for the proton electric form factor. The dashed and dot-dashed curves depict those from the χ QSM and from the Kelly parametrization [27], respectively. The present result is in remarkable agreement with the experimental data in the lower Q^2 region ($Q^2 \leq 0.4$ GeV²). As Q^2 increases, however, it falls off faster than the data. While the sea-quark contribution amounts to only about 5%, it is essential for satisfying the correct normalization of the proton charge. The contribution from the nonlocal part of the EM current is negligible for the proton electric form factor. Figure 3 presents the numerical result for the neutron electric form factor, which is in very good agreement with the experimental data. The present result describes the data noticeably better than the χ QSM, which tends to overestimate $G_E^n(Q^2)$ in the intermediate Q^2 region. In comparison with the Galster-type parametrization given in Ref. [27], the present work provides a better description in the lower Q^2 region

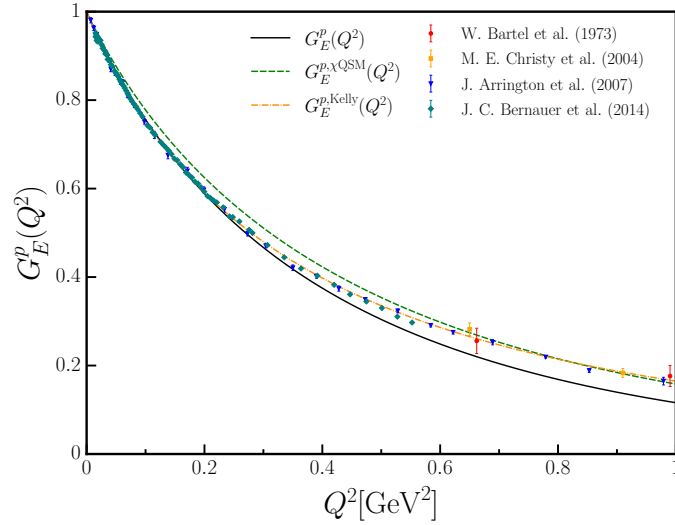


FIG. 2. Electric form factor of the proton. The solid curve depicts the present numerical result for the proton electric form factor, while the dashed and dot-dashed ones represent those obtained from the χ QSM with $M_0 = 420$ MeV [82, 107] and from the Kelly parametrization [27], respectively. The experimental data are taken from Refs. [6–8, 113].

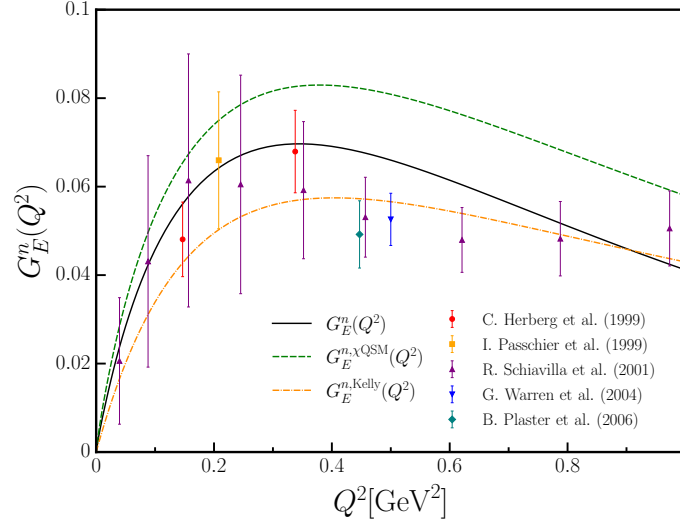


FIG. 3. Electric form factor of the neutron. The solid curve depicts the present numerical result for the neutron electric form factor, while the dashed and dot-dashed ones represent those obtained from the χ QSM with $M_0 = 420$ MeV [82, 107] and from the Galster-type parametrization given in Ref. [27], respectively. The experimental data are taken from Refs. [12, 14, 18, 22, 114].

($Q^2 \leq 0.4 \text{ GeV}^2$), whereas the latter follows the data more closely as Q^2 increases. Nevertheless, both reproduce the overall Q^2 dependence of the data.

In Table III, we list the results for the proton charge radius and the neutron mean-square charge radius. The present result for the proton charge radius is in remarkable agreement with the experimental data, while that for the neutron mean-square charge radius shows reasonable agreement. Both results are in better agreement with experiment than those obtained from the χ QSM.

Figure 4 shows the results for the isoscalar and isovector magnetic form factors of the nucleon, which are defined in Eqs. (49) and (53), respectively. The isoscalar magnetic form factor arises solely from the $1/N_c$ rotational corrections, whereas the isovector one contains both the leading and $1/N_c$ rotational contributions. As expected from this N_c counting, the isovector magnetic form factor dominates over the isoscalar one, as clearly seen in Fig. 4. In Fig. 5, we present the results for the proton magnetic form factor normalized by its magnetic moment. As in the case of the proton electric form factor, the present result describes the experimental data very well in the lower Q^2 region ($Q^2 \lesssim 0.4 \text{ GeV}^2$). As Q^2 increases, however, it falls off faster than the data. Figure 6 shows the results for the

TABLE III. Proton charge radius and neutron mean-square charge radius.

	This work	χ QSM	Experiments [52]
$\sqrt{\langle r^2 \rangle_{\text{ch}}^p}$ [fm]	0.841	0.815	0.8409 ± 0.0004
$\langle r^2 \rangle_{\text{ch}}^n$ [fm ²]	-0.168	-0.219	-0.1155 ± 0.0017

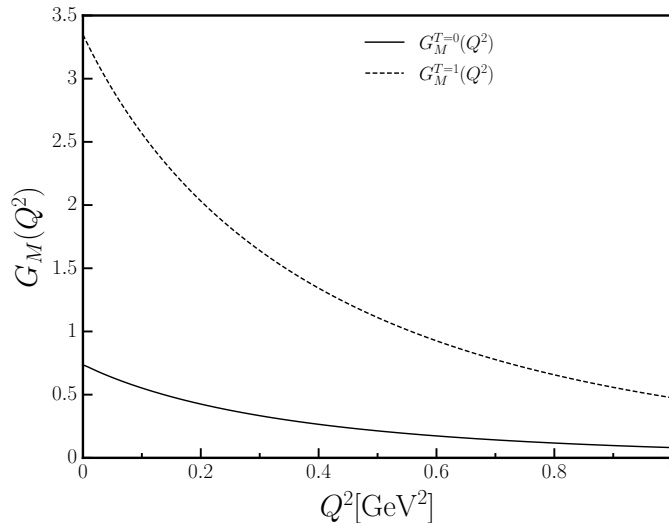


FIG. 4. Isoscalar and isovector magnetic form factors of the nucleon. The solid curve represents the result for the isoscalar magnetic form factor, whereas the dashed one denotes that for the isovector magnetic form factor.

normalized magnetic form factor of the neutron, which turns out to be very similar to the corresponding result from the χ QSM. The Q^2 dependence of the neutron magnetic form factor deviates slightly from the data.

TABLE IV. Magnetic moments of the proton and neutron given in units of the nuclear magneton μ_N . The results from the χ QSM are evaluated with $M_0 = 420$ MeV. The experimental values are taken from Ref. [52], which are rounded to three decimal places.

Quantities	types	This work	χ QSM	Experiments [52]
μ_p	valence	1.724	1.564	-
	sea	0.312	0.378	-
	total	2.042	1.942	2.793
μ_n	valence	-1.015	-0.860	-
	sea	-0.292	-0.455	-
	total	-1.307	-1.315	-1.913

In Table IV, we list the results for the magnetic moments of the proton and neutron in units of the nuclear magneton. It is well known that the magnetic moments of nucleons are underestimated almost by 30% in both the SU(2) [107] and SU(3) [108] χ QSM. Similarly, the present work also yields the underestimated results for the proton and neutron magnetic moments. As shown in Table IV, the valence-quark contributions are dominant over the sea-quark contributions for both the proton and neutron magnetic moments. In Table V, the results for the magnetization

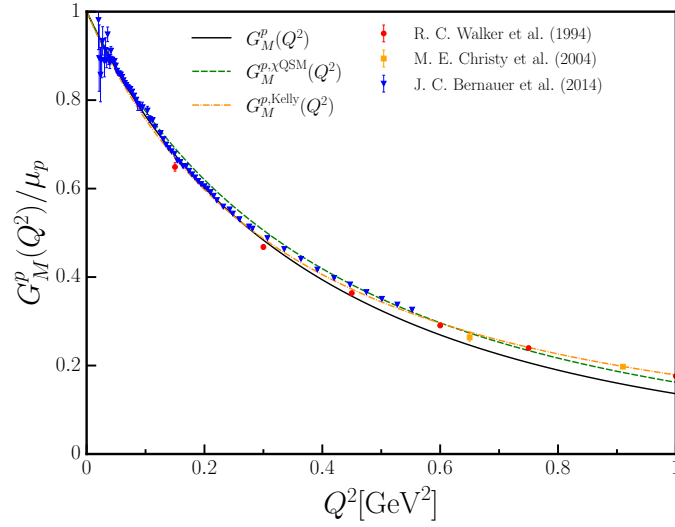


FIG. 5. Magnetic form factor of the proton normalized by its magnetic moment. The solid curve depicts the present numerical result for the proton magnetic form factor, while the dashed and dot-dashed ones represent those obtained from the χ QSM with $M_0 = 420$ MeV [82, 107] and from the Kelly parametrization [27], respectively. The experimental data are taken from Refs. [7, 8, 115].

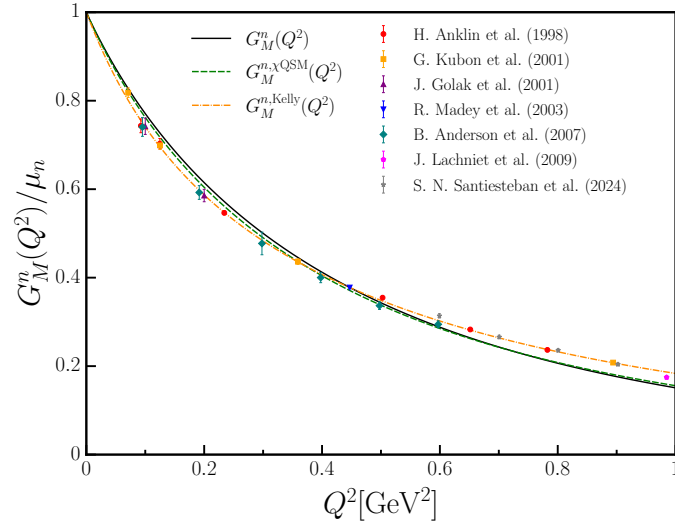


FIG. 6. Magnetic form factor of the neutron normalized by its magnetic moment. The solid curve depicts the present numerical result for the neutron magnetic form factor, while the dashed and dot-dashed ones represent those obtained from the χ QSM with $M_0 = 420$ MeV [82, 107] and from the Kelly parametrization [27], respectively. The experimental data are taken from Refs. [21, 116–121].

TABLE V. Magnetization radii of the proton and neutron. The results from the χ QSM are evaluated with $M_0 = 420$ MeV.

	This work	χ QSM	Experiments [52]
$\sqrt{\langle r^2 \rangle_M^p}$ [fm]	0.832	0.810	0.851 ± 0.026
$\sqrt{\langle r^2 \rangle_M^n}$ [fm]	0.817	0.844	$0.864^{+0.009}_{-0.008}$

radii of the proton and neutron are presented. Both the results are comparable with the experimental data.

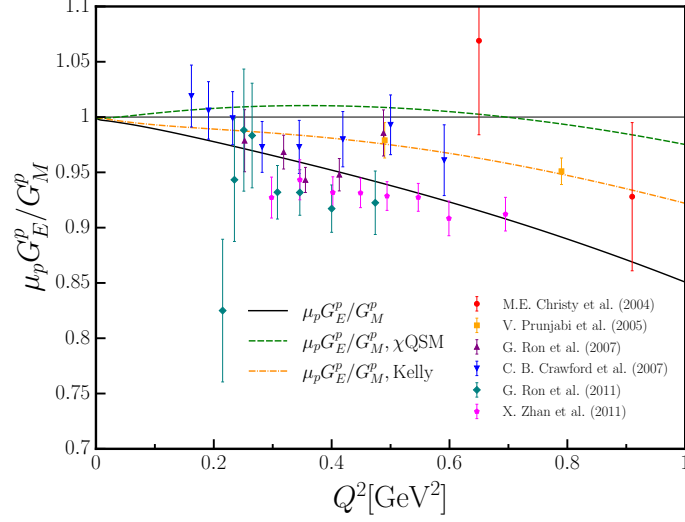


FIG. 7. Ratio of the electric and magnetic form factors G_E and G_M for the proton normalized by its magnetic moment. The solid curve depicts the present numerical result for the ratio, while the dashed and dot-dashed ones represent those obtained from the χ QSM with $M_0 = 420$ MeV [82, 107] and from the Kelly parametrization [27], respectively. The experimental data are taken from Refs. [7, 23–26, 122].

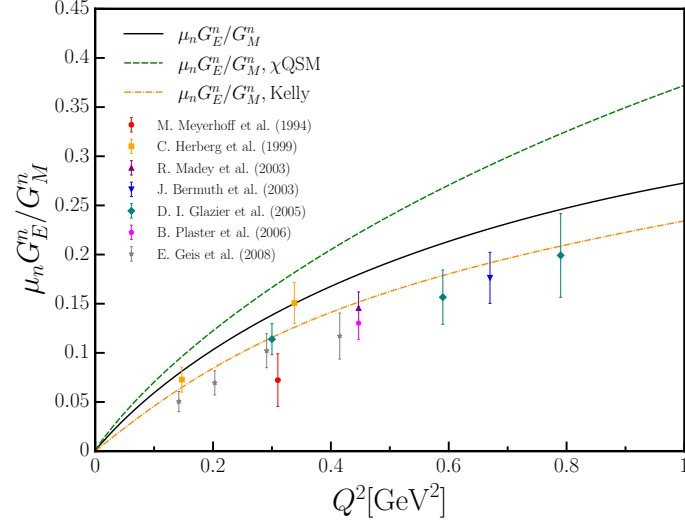


FIG. 8. Ratio of the electric and magnetic form factors G_E and G_M for the neutron normalized by its magnetic moment. The solid curve depicts the present numerical result for the ratio, while the dashed and dot-dashed ones represent those obtained from the χ QSM with $M_0 = 420$ MeV [82, 107] and from the Kelly parametrization [27], respectively. The experimental data are taken from Refs. [9, 12, 17, 19–22].

The experimental data on the EM form factors of the nucleon used for comparison with the present results are based on the Rosenbluth separation method [123], in which the electric and magnetic form factors are extracted separately from the differential cross section of unpolarized electron-proton elastic scattering. With the advent of high-quality polarized electron beams, however, it became possible to extract the electric-to-magnetic form-factor ratio of the proton directly from polarization observables [124]. This ratio carries profound physical implications, since it reflects how differently the electric charge and magnetization are distributed inside the nucleon. As shown in Ref. [24], $\mu_p G_E^p(Q^2)/G_M^p(Q^2)$ exhibits a clear decrease with increasing Q^2 . As displayed in Fig. 7, the present result reproduces this behavior very well, whereas that from the χ QSM first rises slowly and then falls off only mildly. This indicates that the effective chiral theory properly accounts for the spatial difference between the charge and

magnetization distributions inside the nucleon. In Fig. 8, the result for the corresponding neutron ratio appears to be slightly overestimated relative to the data, but still describes them better than the χ QSM does.

V. SUMMARY AND CONCLUSIONS

In the present work, we have investigated the electromagnetic form factors of the nucleon on the basis of an effective chiral theory derived from the QCD instanton vacuum, with the finite current quark mass taken into account. Starting from the improved effective low-energy QCD partition function beyond the chiral limit, the instanton parameters were fixed to $\bar{\rho} = 0.35$ fm and $\bar{R} = 0.86$ fm, and the dynamical quark mass at zero virtuality was determined to be $M_0 = 385$ MeV from the saddle-point equation. Together with the average current quark mass $\bar{m} = 5$ MeV that yields the physical pion mass, all dynamical parameters were fixed without any free adjustment. The momentum-dependent dynamical quark mass arising from the instanton vacuum plays the role of a regulator, so that no additional regularization scheme is required to tame the divergences arising from quark loops.

We first computed the classical nucleon mass and the moment of inertia of the nucleon, and compared them with those obtained within the chiral quark-soliton model and in the chiral limit. The present framework yields $M_{\text{cl}} = 1017$ MeV and $\mathcal{I} = 1.164$ fm, from which the Δ - N mass difference was obtained as $M_{\Delta-N} = 254.2$ MeV. We then evaluated the Sachs electric and magnetic form factors of the proton and neutron, and compared them with the experimental data, the chiral quark-soliton model, and the Kelly parametrization. The isoscalar electric form factor was found to be larger than the isovector one over the entire Q^2 range considered, as expected from the N_c counting. The proton electric form factor was shown to be in remarkable agreement with the experimental data in the lower Q^2 region ($Q^2 \leq 0.4$ GeV²), while it falls off faster than the data as Q^2 increases. The neutron electric form factor was found to be in very good agreement with the experimental data and to describe them noticeably better than the chiral quark-soliton model. The proton charge radius and the neutron mean-square charge radius were obtained as $\sqrt{\langle r^2 \rangle_{\text{ch}}^p} = 0.841$ fm and $\langle r^2 \rangle_{\text{ch}}^n = -0.168$ fm², respectively.

For the magnetic form factors, the isovector contribution was found to dominate over the isoscalar one, as expected from the N_c counting. The proton magnetic form factor normalized by its magnetic moment describes the experimental data well in the lower Q^2 region, while it falls off faster than the data as Q^2 increases. The normalized neutron magnetic form factor turned out to be very similar to that obtained within the chiral quark-soliton model. The magnetic moments of the proton and neutron were obtained as $\mu_p = 2.042$ and $\mu_n = -1.307$ in units of the nuclear magneton, in which the valence-quark contributions dominate over the sea-quark contributions. The magnetization radii of the proton and neutron were also presented and compared with the experimental data.

Finally, we computed the ratios of the electric and magnetic form factors, $\mu_{p,n} G_E^{p,n}(Q^2)/G_M^{p,n}(Q^2)$, and compared them with the polarization-transfer data, the chiral quark-soliton model, and the Kelly parametrization. The proton ratio was shown to reproduce the decreasing behavior with increasing Q^2 observed in the experimental data. The neutron ratio was found to be slightly overestimated relative to the data.

Last but not least, we want to mention that the present effective chiral theory for the structure of the nucleon possesses a natural normalization point given by the inverse of the average instanton size [66, 71, 74, 75], i.e., $\bar{\rho}^{-1} \approx 0.6$ GeV. Interestingly, the present results describe the experimental data very well in the region $Q^2 \leq \bar{\rho}^{-2}$. This indicates that the present theoretical framework is well suited for describing the electromagnetic structure of the nucleon. An important advantage of the present framework is that gluonic observables can be directly computed within it [63, 71]. Corresponding studies are currently under way.

ACKNOWLEDGMENTS

The present work was supported by the National Research Foundation of Korea (NRF) grant funded by the Korea government under Grant RS-2025-00513982 (HChK and HJL) and No. RS-2025-02634319 (YC).

-
- [1] C. F. Perdrisat, V. Punjabi, and M. Vanderhaeghen, *Prog. Part. Nucl. Phys.* **59**, 694 (2007), arXiv:hep-ph/0612014.
 - [2] J. Arrington, K. de Jager, and C. F. Perdrisat, *J. Phys. Conf. Ser.* **299**, 012002 (2011), arXiv:1102.2463 [nucl-ex].
 - [3] V. Punjabi, C. F. Perdrisat, M. K. Jones, E. J. Brash, and C. E. Carlson, *Eur. Phys. J. A* **51**, 79 (2015), arXiv:1503.01452 [nucl-ex].
 - [4] R. Hofstadter, *Rev. Mod. Phys.* **28**, 214 (1956).
 - [5] D. R. Yennie, M. M. Lévy, and D. G. Ravenhall, *Rev. Mod. Phys.* **29**, 144 (1957).

- [6] W. Bartel, F. W. Busser, W. r. Dix, R. Felst, D. Harms, H. Krehbiel, P. E. Kuhlmann, J. McElroy, J. Meyer, and G. Weber, Nucl. Phys. B **58**, 429 (1973).
- [7] M. E. Christy *et al.* (E94110), Phys. Rev. C **70**, 015206 (2004), arXiv:nucl-ex/0401030.
- [8] J. C. Bernauer *et al.* (A1), Phys. Rev. C **90**, 015206 (2014), arXiv:1307.6227 [nucl-ex].
- [9] M. Meyerhoff *et al.*, Phys. Lett. B **327**, 201 (1994).
- [10] T. Eden *et al.*, Phys. Rev. C **50**, R1749 (1994).
- [11] J. Becker *et al.*, Eur. Phys. J. A **6**, 329 (1999).
- [12] C. Herberg *et al.*, Eur. Phys. J. A **5**, 131 (1999).
- [13] M. Ostrick *et al.*, Phys. Rev. Lett. **83**, 276 (1999).
- [14] I. Passchier *et al.*, Phys. Rev. Lett. **82**, 4988 (1999), arXiv:nucl-ex/9907012.
- [15] D. Rohe *et al.*, Phys. Rev. Lett. **83**, 4257 (1999).
- [16] H. Zhu *et al.* (E93026), Phys. Rev. Lett. **87**, 081801 (2001), arXiv:nucl-ex/0105001.
- [17] J. Bermuth *et al.*, Phys. Lett. B **564**, 199 (2003), arXiv:nucl-ex/0303015.
- [18] G. Warren *et al.* (Jefferson Lab E93-026), Phys. Rev. Lett. **92**, 042301 (2004), arXiv:nucl-ex/0308021.
- [19] D. I. Glazier *et al.*, Eur. Phys. J. A **24**, 101 (2005), arXiv:nucl-ex/0410026.
- [20] E. Geis *et al.* (BLAST), Phys. Rev. Lett. **101**, 042501 (2008), arXiv:0803.3827 [nucl-ex].
- [21] R. Madey *et al.* (E93-038), Phys. Rev. Lett. **91**, 122002 (2003), arXiv:nucl-ex/0308007.
- [22] B. Plaster *et al.* (Jefferson Laboratory E93-038), Phys. Rev. C **73**, 025205 (2006), arXiv:nucl-ex/0511025.
- [23] C. B. Crawford *et al.*, Phys. Rev. Lett. **98**, 052301 (2007), arXiv:nucl-ex/0609007.
- [24] G. Ron *et al.*, Phys. Rev. Lett. **99**, 202002 (2007), arXiv:0706.0128 [nucl-ex].
- [25] G. Ron *et al.* (Jefferson Lab Hall A), Phys. Rev. C **84**, 055204 (2011), arXiv:1103.5784 [nucl-ex].
- [26] X. Zhan *et al.*, Phys. Lett. B **705**, 59 (2011), arXiv:1102.0318 [nucl-ex].
- [27] J. J. Kelly, Phys. Rev. C **70**, 068202 (2004).
- [28] W. M. Alberico, S. M. Bilenky, C. Giunti, and K. M. Graczyk, Phys. Rev. C **79**, 065204 (2009), arXiv:0812.3539 [hep-ph].
- [29] I. A. Qattan and J. Arrington, Phys. Rev. C **86**, 065210 (2012), arXiv:1209.0683 [nucl-ex].
- [30] S. Capitani, M. Della Morte, D. Djukanovic, G. von Hippel, J. Hua, B. Jäger, B. Knippschild, H. B. Meyer, T. D. Rae, and H. Wittig, Phys. Rev. D **92**, 054511 (2015), arXiv:1504.04628 [hep-lat].
- [31] Y.-C. Jang, R. Gupta, H.-W. Lin, B. Yoon, and T. Bhattacharya, Phys. Rev. D **101**, 014507 (2020), arXiv:1906.07217 [hep-lat].
- [32] C. Alexandrou, S. Bacchio, M. Constantinou, J. Finkenrath, K. Hadjiyiannakou, K. Jansen, G. Koutsou, and A. Vaquero Aviles-Casco, Phys. Rev. D **100**, 014509 (2019), arXiv:1812.10311 [hep-lat].
- [33] C. Alexandrou, S. Bacchio, G. Koutsou, B. Prasad, and G. Spanoudes, (2025), arXiv:2507.20910 [hep-lat].
- [34] R. Pohl *et al.*, Nature **466**, 213 (2010).
- [35] A. Antognini *et al.*, Science **339**, 417 (2013).
- [36] M. Horbatsch and E. A. Hessels, Phys. Rev. C **93**, 015204 (2016), arXiv:1509.05644 [nucl-ex].
- [37] J. Arrington and I. Sick, J. Phys. Chem. Ref. Data **44**, 031204 (2015), arXiv:1505.02680 [nucl-ex].
- [38] D. W. Higinbotham, A. A. Kabir, V. Lin, D. Meekins, B. Norum, and B. Sawatzky, Phys. Rev. C **93**, 055207 (2016), arXiv:1510.01293 [nucl-ex].
- [39] H. Fleurbaey, S. Galtier, S. Thomas, M. Bonnaud, L. Julien, F. Biraben, F. Nez, M. Abgrall, and J. Guéna, Phys. Rev. Lett. **120**, 183001 (2018), arXiv:1801.08816 [physics.atom-ph].
- [40] N. Bezzin, T. Valdez, M. Horbatsch, A. Marsman, A. C. Vutha, and E. A. Hessels, Science **365**, 1007 (2019).
- [41] W. Xiong *et al.*, Nature **575**, 147 (2019).
- [42] A. Grinin, A. Matveev, D. C. Yost, L. Maisenbacher, V. Wirthl, R. Pohl, T. W. Hänsch, and T. Udem, Science **370**, abc7776 (2020).
- [43] H. Atac, M. Constantinou, Z. E. Meziani, M. Paolone, and N. Sparveris, Nature Commun. **12**, 1759 (2021), arXiv:2103.10840 [nucl-ex].
- [44] A. D. Brandt, S. F. Cooper, C. Rasor, Z. Burkley, D. C. Yost, and A. Matveev, Phys. Rev. Lett. **128**, 023001 (2022), arXiv:2111.08554 [physics.atom-ph].
- [45] S. Scheidegger and F. Merkt, Phys. Rev. Lett. **132**, 113001 (2024).
- [46] P. J. Mohr, D. B. Newell, B. N. Taylor, and E. Tiesinga, Rev. Mod. Phys. **97**, 025002 (2025), arXiv:2409.03787 [hep-ph].
- [47] L. Maisenbacher, V. Wirthl, A. Matveev, A. Grinin, R. Pohl, T. W. Hänsch, and T. Udem, Nature **650**, 845 (2026), arXiv:2602.14980 [physics.atom-ph].
- [48] R. Pohl, R. Gilman, G. A. Miller, and K. Pachucki, Ann. Rev. Nucl. Part. Sci. **63**, 175 (2013), arXiv:1301.0905 [physics.atom-ph].
- [49] H. Gao and M. Vanderhaeghen, Rev. Mod. Phys. **94**, 015002 (2022), arXiv:2105.00571 [hep-ph].
- [50] A. Antognini, F. Hagelstein, and V. Pascalutsa, Ann. Rev. Nucl. Part. Sci. **72**, 389 (2022), arXiv:2205.10076 [nucl-th].
- [51] K. Nakamura *et al.* (Particle Data Group), J. Phys. G **37**, 075021 (2010).
- [52] S. Navas *et al.* (Particle Data Group), Phys. Rev. D **110**, 030001 (2024).
- [53] D. Müller, D. Robaschik, B. Geyer, F. M. Dittes, and J. Hořejši, Fortsch. Phys. **42**, 101 (1994), arXiv:hep-ph/9812448.
- [54] X.-D. Ji, Phys. Rev. D **55**, 7114 (1997), arXiv:hep-ph/9609381.
- [55] A. V. Radyushkin, Phys. Lett. B **385**, 333 (1996), arXiv:hep-ph/9605431.
- [56] K. Goeke, M. V. Polyakov, and M. Vanderhaeghen, Prog. Part. Nucl. Phys. **47**, 401 (2001), arXiv:hep-ph/0106012.
- [57] M. Diehl, Phys. Rept. **388**, 41 (2003), arXiv:hep-ph/0307382.
- [58] G. A. Miller, Phys. Rev. Lett. **99**, 112001 (2007), arXiv:0705.2409 [nucl-th].

- [59] C. Lorcé, Phys. Rev. Lett. **125**, 232002 (2020), arXiv:2007.05318 [hep-ph].
- [60] J.-Y. Kim and H.-C. Kim, Phys. Rev. D **104**, 074003 (2021), arXiv:2106.10986 [hep-ph].
- [61] E. Leader and C. Lorcé, Phys. Rept. **541**, 163 (2014), arXiv:1309.4235 [hep-ph].
- [62] C. Lorcé, Phys. Lett. B **735**, 344 (2014), arXiv:1401.7784 [hep-ph].
- [63] J.-Y. Kim, H.-Y. Won, H.-C. Kim, and C. Weiss, Phys. Rev. D **110**, 054026 (2024), arXiv:2403.07186 [hep-ph].
- [64] E. V. Shuryak, Nucl. Phys. B **203**, 93 (1982).
- [65] D. Diakonov and V. Y. Petrov, Nucl. Phys. B **245**, 259 (1984).
- [66] D. Diakonov and V. Y. Petrov, Nucl. Phys. B **272**, 457 (1986).
- [67] T. Schäfer and E. V. Shuryak, Rev. Mod. Phys. **70**, 323 (1998), arXiv:hep-ph/9610451.
- [68] D. Diakonov, Prog. Part. Nucl. Phys. **51**, 173 (2003), arXiv:hep-ph/0212026.
- [69] W.-Y. Liu, (2025), arXiv:2501.07776 [hep-ph].
- [70] M. A. Shifman, A. I. Vainshtein, and V. I. Zakharov, Nucl. Phys. B **147**, 385 (1979).
- [71] D. Diakonov, M. V. Polyakov, and C. Weiss, Nucl. Phys. B **461**, 539 (1996), arXiv:hep-ph/9510232.
- [72] H.-C. Kim, M. M. Musakhanov, and M. Siddikov, Phys. Lett. B **633**, 701 (2006), arXiv:hep-ph/0508211.
- [73] K. Goeke, H.-C. Kim, M. M. Musakhanov, and M. Siddikov, Phys. Rev. D **76**, 116007 (2007), arXiv:0708.3526 [hep-ph].
- [74] H.-C. Kim, M. V. Polyakov, and K. Goeke, Phys. Rev. D **53**, 4715 (1996), arXiv:hep-ph/9509283.
- [75] M. V. Polyakov and H.-D. Son, Phys. Rev. D **102**, 114005 (2020), arXiv:2008.06270 [hep-ph].
- [76] M. Musakhanov, Eur. Phys. J. C **9**, 235 (1999), arXiv:hep-ph/9810295.
- [77] M. Musakhanov, Nucl. Phys. A **699**, 340 (2002).
- [78] Y. Choi and H.-C. Kim, Phys. Rev. D **111**, 074023 (2025), arXiv:2501.12114 [hep-ph].
- [79] D. Diakonov, V. Y. Petrov, and P. V. Pobylitsa, Nucl. Phys. B **306**, 809 (1988).
- [80] M. Wakamatsu and H. Yoshiki, Nucl. Phys. A **524**, 561 (1991).
- [81] A. Blotz, D. Diakonov, K. Goeke, N. W. Park, V. Petrov, and P. V. Pobylitsa, Nucl. Phys. A **555**, 765 (1993).
- [82] C. V. Christov, A. Blotz, H.-C. Kim, P. Pobylitsa, T. Watabe, T. Meissner, E. Ruiz Arriola, and K. Goeke, Prog. Part. Nucl. Phys. **37**, 91 (1996), arXiv:hep-ph/9604441.
- [83] D. Diakonov, in *Advanced Summer School on Nonperturbative Quantum Field Physics* (1997) pp. 1–55, arXiv:hep-ph/9802298.
- [84] E. Witten, Nucl. Phys. B **160**, 57 (1979).
- [85] E. Witten, Nucl. Phys. B **223**, 422 (1983).
- [86] E. Witten, Nucl. Phys. B **223**, 433 (1983).
- [87] G. S. Adkins and C. R. Nappi, Nucl. Phys. B **233**, 109 (1984).
- [88] R. G. Sachs, Phys. Rev. **126**, 2256 (1962).
- [89] M. Chretien and R. E. Peierls, Proc. Roy. Soc. Lond. A **223**, 468 (1954).
- [90] B. Holdom, J. Terning, and K. Verbeek, Phys. Lett. B **232**, 351 (1989).
- [91] B. Holdom, J. Terning, and K. Verbeek, Phys. Lett. B **245**, 612 (1990).
- [92] J. W. Bos, J. H. Koch, and H. W. L. Naus, Phys. Rev. C **44**, 485 (1991).
- [93] B. Holdom, Phys. Rev. D **45**, 2534 (1992).
- [94] R. D. Ball and G. Ripka, in *Conference on Many-Body Physics* (1993) pp. 129–140, arXiv:hep-ph/9312260.
- [95] R. D. Bowler and M. C. Birse, Nucl. Phys. A **582**, 655 (1995), arXiv:hep-ph/9407336.
- [96] B. Golli, W. Broniowski, and G. Ripka, Phys. Lett. B **437**, 24 (1998), arXiv:hep-ph/9807261.
- [97] W. Broniowski, in *Mini-Workshop Bled 1999: Hadrons as Solitons* (1999) pp. 17–26, arXiv:hep-ph/9909438.
- [98] P. V. Pobylitsa, Phys. Lett. B **226**, 387 (1989).
- [99] M. M. Musakhanov and H.-C. Kim, Phys. Lett. B **572**, 181 (2003), arXiv:hep-ph/0206233.
- [100] H.-C. Kim, M. Musakhanov, and M. Siddikov, Phys. Lett. B **608**, 95 (2005), arXiv:hep-ph/0411181.
- [101] S.-i. Nam and H.-C. Kim, Phys. Rev. D **74**, 076005 (2006), arXiv:hep-ph/0609267.
- [102] S.-i. Nam and H.-C. Kim, Phys. Rev. D **75**, 094011 (2007), arXiv:hep-ph/0703089.
- [103] S.-i. Nam and H.-C. Kim, Phys. Rev. D **77**, 094014 (2008), arXiv:0709.1745 [hep-ph].
- [104] H.-D. Son, S.-i. Nam, and H.-C. Kim, Phys. Lett. B **747**, 460 (2015), arXiv:1502.01558 [hep-ph].
- [105] S.-I. Shim and H.-C. Kim, Phys. Lett. B **772**, 687 (2017), arXiv:1704.03263 [hep-ph].
- [106] S.-I. Shim, A. Hosaka, and H.-C. Kim, Phys. Lett. B **795**, 438 (2019), arXiv:1810.06815 [hep-ph].
- [107] C. V. Christov, A. Z. Gorski, K. Goeke, and P. V. Pobylitsa, Nucl. Phys. A **592**, 513 (1995), arXiv:hep-ph/9507256.
- [108] H.-C. Kim, A. Blotz, M. V. Polyakov, and K. Goeke, Phys. Rev. D **53**, 4013 (1996), arXiv:hep-ph/9504363.
- [109] W. Broniowski, B. Golli, and G. Ripka, Nucl. Phys. A **703**, 667 (2002), arXiv:hep-ph/0107139.
- [110] K. Goeke, M. M. Musakhanov, and M. Siddikov, Phys. Rev. D **76**, 076007 (2007), arXiv:0707.1997 [hep-ph].
- [111] S. Kahana and G. Ripka, Nucl. Phys. A **429**, 462 (1984).
- [112] G. S. Adkins, C. R. Nappi, and E. Witten, Nucl. Phys. B **228**, 552 (1983).
- [113] J. Arrington, W. Melnitchouk, and J. A. Tjon, Phys. Rev. C **76**, 035205 (2007), arXiv:0707.1861 [nucl-ex].
- [114] R. Schiavilla and I. Sick, Phys. Rev. C **64**, 041002 (2001), arXiv:nucl-ex/0107004.
- [115] R. C. Walker *et al.*, Phys. Rev. D **49**, 5671 (1994).
- [116] H. Anklin *et al.*, Phys. Lett. B **428**, 248 (1998).
- [117] G. Kubon *et al.*, Phys. Lett. B **524**, 26 (2002), arXiv:nucl-ex/0107016.
- [118] J. Golak, G. Ziemer, H. Kamada, H. Witala, and W. Gloeckle, Phys. Rev. C **63**, 034006 (2001), arXiv:nucl-th/0008008.
- [119] B. Anderson *et al.* (Jefferson Lab E95-001), Phys. Rev. C **75**, 034003 (2007), arXiv:nucl-ex/0605006.
- [120] J. Lachniet *et al.* (CLAS), Phys. Rev. Lett. **102**, 192001 (2009), arXiv:0811.1716 [nucl-ex].

- [121] S. N. Santiesteban *et al.* (Jefferson Lab Hall A), Phys. Rev. Lett. **132**, 162501 (2024), arXiv:2304.13770 [nucl-ex].
- [122] V. Punjabi *et al.*, Phys. Rev. C **71**, 055202 (2005), [Erratum: Phys.Rev.C 71, 069902 (2005)], arXiv:nucl-ex/0501018.
- [123] M. N. Rosenbluth, Phys. Rev. **79**, 615 (1950).
- [124] M. K. Jones *et al.* (Jefferson Lab Hall A), Phys. Rev. Lett. **84**, 1398 (2000), arXiv:nucl-ex/9910005.